Available online at www.sciencedirect.com
SCIENCE DIRECT®
Journal of Solid State Chemistry 176 (2003) 266–272
JOURNAL OF SOLID STATE CHEMISTRY
http://elsevier.com/locate/jssc

Magnetic properties of ternary sodium oxides $NaLnO_2$ (Ln = rare earths)

Yuta Hashimoto, Makoto Wakeshima, and Yukio Hinatsu*

Division of Chemistry, Graduate School of Science, Hokkaido University, Sapporo 060-0810, Japan

Received 30 April 2003; received in revised form 27 July 2003; accepted 1 August 2003

Abstract

Magnetic properties of ternary sodium oxides $NaLnO_2$ (Ln = rare earths) are investigated. Their crystal structures are grouped into three types of structures, which are α-$LiFeO_2$, β-$LiFeO_2$, and α-$NaFeO_2$, depending on the size of rare earths. Their magnetic susceptibilities and specific heats have been measured from 1.8 to 300 K. Among them, $NaGdO_2$, $NaDyO_2$, and $NaHoO_2$ show antiferromagnetic transitions at 2.4, 2.2, and 2.4 K, respectively, and $NaNdO_2$ transforms to the ferromagnetic state below 2.4 K. $NaSmO_2$, $NaErO_2$, and $NaYbO_2$ exhibit a magnetic anomaly below 1.8 K.

Keywords: Magnetic properties; Rare earths; Oxides; Specific heat; Magnetic susceptibility

1. Introduction

The most stable oxidation state of lanthanide (Ln) ions is trivalent, and the electronic configuration of Ln^{3+} ions is [Xe] $4f^n$ ([Xe]: xenon electronic core). Their magnetic properties are determined by the unpaired $4f$ electrons. They are highly localized electrons, and the orbital contributions to their magnetic moments are significant. These features are in contrast with those of d electrons: the d orbitals are located in the valency shell and their contributions to the magnetic moments are essentially quenched. Generally, the shielding by the surrounding $5s$ and $5p$ electrons in the outer shell makes the magnetic interactions between $4f$ electrons in the condensed matter very weak, compared with those between d electrons. In fact, many of the lanthanide oxides order magnetically at <4 K. Among many magnetic studies on oxides containing lanthanide ions, the magnetic properties of alkali-metal lanthanide oxides are limited, because of the difficulty in preparing these oxides [1].

It is known that crystal structures of ternary alkali-metal rare earth oxides $MLnO_2$ (M = alkali metals, Ln = rare earths) have various types depending on the alkali metal and rare earth ionic radii [2]. The crystal structures of $LiLnO_2$ have been grouped into four types (α,β,γ,δ-types) [3]. In the α- and β-type structures, the Ln^{3+} ions are coordinated by six oxide ions and each LnO_6 octahedron shares four edges and four corners with the surrounding LnO_6 octahedra. The α-type structure is tetragonal (space group; $I4_1/amd$), while the β-type structure is distorted to a monoclinic structure with the space group of $P2_1/c$. In the series of $LiLnO_2$ compounds, we have found that the Dy, Ho, Y, and Er compounds showed a structural transition from the α-type (high-temperature phase) to the β-type (low-temperature phase) at 475, 360, 325, and 200 K, respectively, and that the antiferromagnetic orderings of the R^{3+} ions have been observed for the Sm, Gd, Dy, and Er compounds below 1.9, 2.5, 3.0, and 4.2 K, respectively [4].

For a series of sodium rare earth oxides $NaLnO_2$, their crystal structures are grouped into three types, depending on the Ln^{3+} ionic radius. These structures are typified by other compounds, which are α-$LiFeO_2$ type (space group: $I4_1/amd$), β-$LiFeO_2$ type (space group: $C2/c$), and α-$NaFeO_2$ type (space group:$R\bar{3}m$) [5]. The α-$NaFeO_2$ is isostructural with α-$LiRO_2$. All the compounds have an ordered rocksalt lattice. If the ionic radius of the Ln^{3+} ion is larger than that of the Na^+ ion (La^{3+} up to Gd^{3+}), the α-$LiFeO_2$ structure is found. This structure is tetragonal and has a unit cell twice as large as that of the statistical rocksalt structure. If the

*Corresponding author. Fax: +81-11-706-2702.
E-mail address: hinatsu@sci.hokudai.ac.jp (Y. Hinatsu).

0022-4596/$ - see front matter © 2003 Elsevier Inc. All rights reserved.
doi:10.1016/j.jssc.2003.08.001

Ln^{3+} ion is a little smaller than Na^{+} (Tb^{3+} up to Er^{3+}), an X-ray pattern of β-$LiFeO_2$ type is found. The crystal structure for $NaLnO_2$ has been determined by Gondrand et al. [6] and Hoppe et al. [1,2]. If the Ln^{3+} ion is considerably smaller than Na^{+} (Tm^{3+} up to Lu^{3+}, including Y^{3+}, Sc^{3+}), the hexagonal α-$NaFeO_2$ structure is found. In this structure, the (111) cation layers are occupied alternatively by Na^{+} and Ln^{3+} ions.

In this study, we have paid attention to the structural and magnetic properties of ternary sodium oxides $NaLnO_2$. Some interesting magnetic anomalies have been found at low temperatures through magnetic susceptibility, magnetization, and specific heat measurements, and their results are discussed here.

2. Experimental

Samples were prepared by the solid state reaction. As starting materials, Ln_2O_3 (Ln = La–Nd, Sm–Lu), Na_2CO_3 (for Eu–Lu), and $NaNO_3$ (for La–Nd and Sm) were used. These reagents were weighed in the $Na/Ln = 1.2$ metal ratios to prevent loss of sodium from evaporation, and ground in an agate mortar. The mixtures were pelletized and heated in air at 1273 K (Ln = La–Nd, Sm–Er) or 1173 K (Ln = Tm–Lu) for 12–48 h with some addition of Na_2CO_3 or $NaNO_3$ and several regrindings. As will be described later, we could obtain two kinds of $NaErO_2$ specimens with different crystal structures, i.e., β-$LiFeO_2$ and α-$NaFeO_2$ types. The $NaErO_2$ with the β-$LiFeO_2$ type structure was prepared by heating the mixtures of Er_2O_3 and Na_2CO_3 at 1273 K and cooling them slowly in a furnace. The other $NaErO_2$ specimen with the α-$NaFeO_2$ type structure (the high-temperature phase) was prepared by quenching the mixtures of Er_2O_3 and Na_2CO_3 from 1273 K to room temperature.

Powder X-ray diffraction profiles were measured using a Rigaku Multi-Flex diffractometer with Cu$K\alpha$ radiation equipped with a curved graphite monochromator. The data were collected by step scanning in the angle range $10° \leqslant 2\theta \leqslant 120°$ at a 2θ step size of 0.04°.

The temperature dependence of the magnetic susceptibility was measured with a SQUID magnetometer (Quantum Design, MPMS) under both zero-field-cooled conditions (ZFC) and field-cooled conditions (FC). The former was measured on heating the sample to 300 K under the applied magnetic field of 0.1 T after zero-field cooling to 1.8 K. The latter was measured upon cooling the sample from 10 to 1.8 K under 0.1 T. The magnetization was measured with a physical property measuring system (Quantum Design, PPMS) by changing the applied magnetic field from 0 to 9 T.

The specific heats were measured using a relaxation technique applied by a specific heat measuring system (Quantum Design, PPMS) in the temperature range of $1.8 \leqslant T \leqslant 300$ K. The sample in the form of a thin plate was mounted on a sample holder with apiezon for better thermal contact.

3. Results and discussion

3.1. Crystal structures

The $NaLnO_2$ compounds were obtained as a single phase except for the case of Ln = La, Pr, and Tb, although very small amount of impurities (which are unreacted Na_2O or Ln_2O_3) is detected. From the powder X-ray diffraction patterns, their crystal structures are grouped into following three structural types:

Ln = Nd, Sm−Gd : α-$LiFeO_2$ type (space group : $I4_1/amd$),

Ln = Dy−Er : β-$LiFeO_2$ type (space group : $C2/c$),

Ln = Er−Lu : α-$NaFeO_2$ type (space group : $R\bar{3}m$).

Fig. 1 shows the typical powder X-ray diffraction patterns for the three types of compounds, $NaGdO_2$ (α-$LiFeO_2$ type), $NaErO_2$ (β-$LiFeO_2$ type), and $NaErO_2$ (α-$NaFeO_2$ type). For $NaErO_2$, we could obtain two

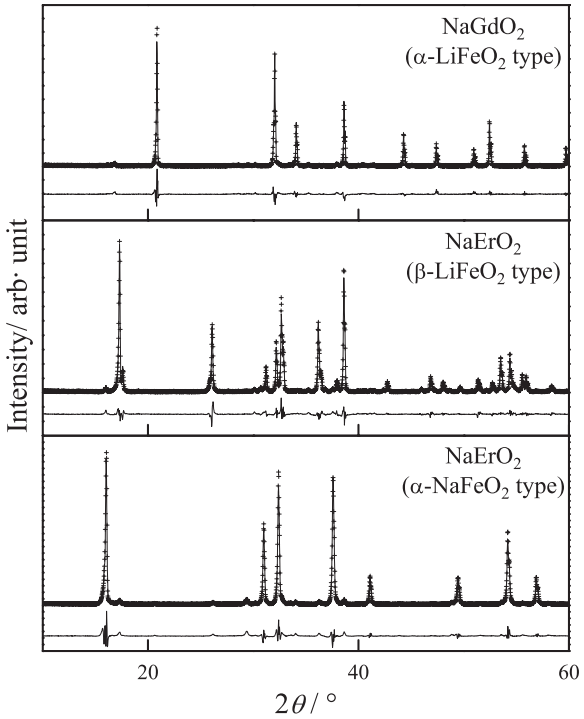

Fig. 1. Powder X-ray diffraction patterns for $NaGdO_2$ (α-$LiFeO_2$ type), $NaErO_2$ (β-$LiFeO_2$ type), and $NaErO_2$ (α-$NaFeO_2$ type). The calculated and observed profiles are shown on the top, solid line and cross markers, respectively. The lower trace is a plot of the difference between calculated and observed intensities.

Table 1
Lattice parameters and reliability factors for $NaRO_2$ determined by X-ray diffraction measurements

Compounds	Structure	a (Å)	b (Å)	c (Å)	β (deg)	R_{wp} (%)	R_I (%)
$NaNdO_2$	α-$LiFeO_2$	4.7411(8)	—	10.8661(10)	—	15.22	3.60
$NaSmO_2$	α-$LiFeO_2$	4.6981(8)	—	10.6565(10)	—	19.52	5.95
$NaEuO_2$	α-$LiFeO_2$	4.6827(9)	—	10.5728(9)	—	26.70	6.82
$NaGdO_2$	α-$LiFeO_2$	4.6607(8)	—	10.5191(9)	—	19.30	5.03
$NaDyO_2$	β-$LiFeO_2$	10.4321(9)	13.2659(8)	6.0728(6)	146.779(14)	19.50	7.39
$NaHoO_2$	β-$LiFeO_2$	9.9848(9)	13.2027(8)	6.0488(6)	146.748(13)	12.54	3.02
$NaErO_2$	β-$LiFeO_2$	9.9243(12)	13.1369(7)	6.0216(7)	146.713(14)	15.97	3.88
$NaErO_2$	α-$NaFeO_2$	3.3842(7)	—	16.5945(15)	—	15.62	3.48
$NaTmO_2$	α-$NaFeO_2$	3.3703(7)	—	16.5311(13)	—	12.42	2.11
$NaYbO_2$	α-$NaFeO_2$	3.3510(6)	—	16.5253(12)	—	15.35	2.65
$NaLuO_2$	α-$NaFeO_2$	3.3518(6)	—	16.5300(12)	—	15.26	1.83

Note: $R_{wp} = [\sum_i w_i(y_i - f_i(x))^2/\sum_i w_i y_i^2]^{1/2}$ and $R_I = \sum|I_k(o) - I_k(c)|/\sum I_k(o)$.

Table 2
Atomic positional parameters for $NaGdO_2$ (α-$LiFeO_2$ type), $NaErO_2$ (β-$LiFeO_2$ type) and $NaErO_2$ (α-$NaFeO_2$ type)

Atom	Site	x	y	z	B (Å^2)
$NaGdO_2$ (α-$LiFeO_2$ type)		Space group: $I4_1/amd$			
Na	4*b*	0	0	1/2	0.4
Gd	4*a*	0	0	0	0.4
O	8*e*	0	0	0.219(1)	0.6
$NaErO_2$ (β-$LiFeO_2$ type)		Space group: $C2/c$			
Na(1)	4*e*	0	0.572(2)	1/4	0.4
Na(2)	4*e*	0	0.811(2)	1/4	0.4
Er(1)	4*e*	0	0.057(1)	1/4	0.4
Er(2)	4*e*	0	0.317(1)	1/4	0.4
O(1)	8*f*	0.234(2)	0.057(2)	0.256(3)	0.6
O(2)	8*f*	0.256(2)	0.307(2)	0.308(3)	0.6
$NaErO_2$ (α-$NaFeO_2$ type)		Space group: $R\bar{3}m$			
Na	3*b*	0	0	1/2	0.67(50)
Er	3*a*	0	0	0	0.25(12)
O	6*c*	0	0	0.264(4)	0.24(20)

kinds of specimens with different crystal structures, β-$LiFeO_2$ and α-$NaFeO_2$ types. We have performed the Rietveld analysis with the program RIETAN-97 [7] for the diffraction profiles. Table 1 lists the lattice parameters and reliability factors for the $NaLnO_2$ compounds prepared in this study, and Table 2 lists the atomic positional parameters for the above three types of compounds. For the compounds with the same crystal structure, the lattice parameters decrease with decreasing the ionic radius of the Ln^{3+} ion.

3.2. Magnetic properties

3.2.1. Magnetic susceptibilities

The temperature dependence of the magnetic susceptibilities (χ) was measured in the temperature range of 1.8–300 K for all the $NaLnO_2$ compounds except for the nonmagnetic compound with Ln = Lu.

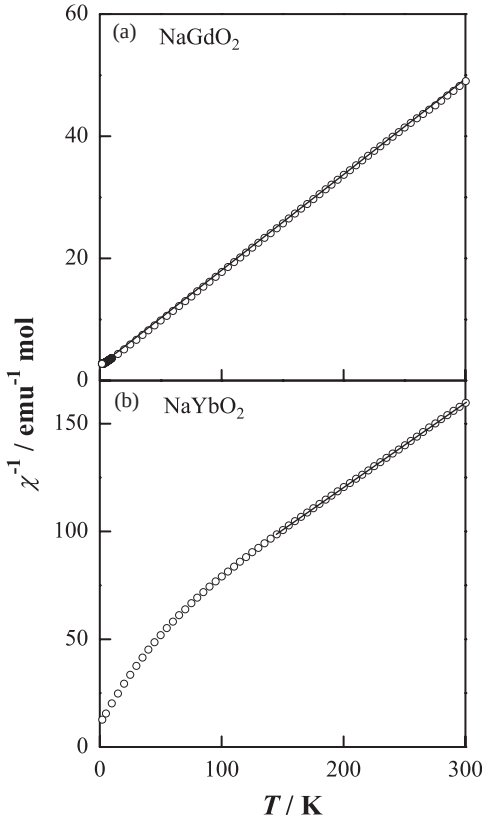

Fig. 2. Temperature dependence of the reciprocal magnetic susceptibilities for (a) $NaGdO_2$ and (b) $NaYbO_2$. The solid straight lines show the Curie–Weiss fittings (see text).

Figs. 2 (a) and (b) show the temperature dependence of the reciprocal magnetic susceptibilities for $NaGdO_2$ and $NaYbO_2$. The reciprocal susceptibilities of $NaYbO_2$ exhibit the Curie–Weiss behavior between 150 and 300 K, but deviate from the Curie–Weiss law below 150 K, while those of $NaGdO_2$ obey the Curie–Weiss law in the whole experimental temperature range. The Gd^{3+} ion has the $^8S_{7/2}$ ground state without the orbital momentum, so the crystal field does not affect the susceptibility of the Gd^{3+} ions. On the other hand, the

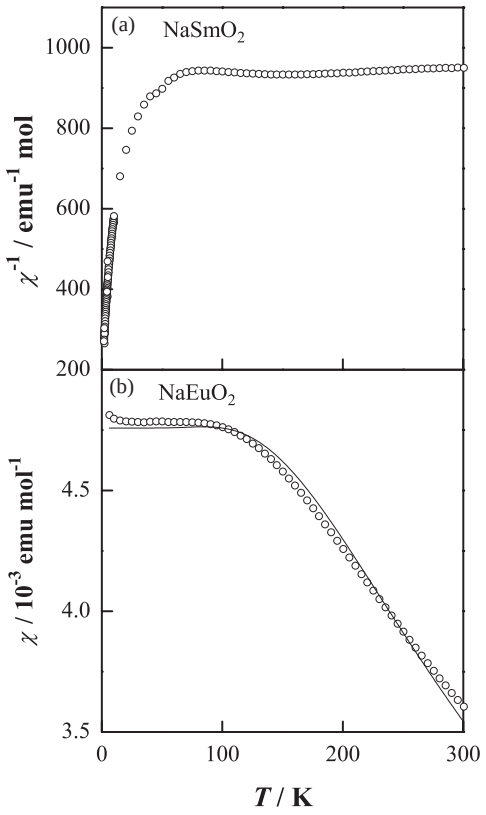

Fig. 3. (a) Temperature dependence of the reciprocal magnetic susceptibilities for $NaSmO_2$. (b) Temperature dependence of the magnetic susceptibility for $NaEuO_2$. The solid line is the calculation results by Eq. (1) (see text).

$^2F_{7/2}$ ground state of the Yb^{3+} ion should be split into four doublets in the tetragonal symmetry. The large deviation from the Curie–Weiss law below 150 K is attributable to this crystal field effect on the Yb^{3+} ion. The magnetic susceptibility of all the $NaLnO_2$ compounds, except for $NaSmO_2$ and $NaEuO_2$, obeys the Curie–Weiss law above at least 150 K.

For $NaSmO_2$ and $NaEuO_2$, the spacings of the multiplet levels for the Sm^{3+} and Eu^{3+} ions are not large compared to k_BT (k_B: Boltzmann constant), so the magnetic susceptibility should take into consideration the excited states. Figs. 3(a) and (b) shows the temperature dependence of the magnetic susceptibilities for $NaSmO_2$ and $NaEuO_2$, respectively. The susceptibility plateau of $NaEuO_2$ below 100 K in Fig. 3(b) is attributed to the temperature-independent term of the Van Vleck formula by the population to the nonmagnetic ground state ($^7F_0$). Considering the contribution of the excited states ^7F_J ($J = 1, 2, \ldots, 6$), the molar magnetic susceptibility for Eu^{3+} can be written by the following equation [8],

$$\chi(\mathrm{Eu}^{3+}) = \frac{N_A\mu_B^2/3k_B}{\gamma T} \times \frac{24 + (13.5\gamma - 1.5)e^{-\gamma} + (67.5\gamma - 2.5)e^{-3\gamma} + (189\gamma - 3.5)e^{-6\gamma} + \cdots}{1 + 3e^{-\gamma} + 5e^{-3\gamma} + 7e^{-6\gamma} + \cdots}, \quad (1)$$

Table 3
Magnetic properties of $NaLnO_2$

Ln	Structure	Magnetic properties	θ/K	μ_{eff}	
				Obs. (μ_B)	Cal. (μ_B)
Nd	α-$LiFeO_2$	Ferro $T_C = 2.4$ K	2.53	3.49	3.62
Sm	α-$LiFeO_2$	Anomaly ($T_N < 1.8$ K)	—	1.59[a]	1.55[b]
Eu	α-$LiFeO_2$	Para	—	3.25[a]	3.40[b]
Gd	α-$LiFeO_2$	Antiferro $T_N = 2.4$ K	−23.4	7.59	7.94
Dy	β-$LiFeO_2$	Antiferro $T_N = 2.2$ K	−29.4	10.00	10.63
Ho	β-$LiFeO_2$	Antiferro $T_N = 2.4$ K	−37.9	10.08	10.58
Er	β-$LiFeO_2$	Anomaly ($T_N < 1.8$ K)	−19.1	8.75	9.59
Er	α-$NaFeO_2$	Para	−21.5	9.08	9.59
Tm	α-$NaFeO_2$	Para	−47.5	7.14	7.55
Yb	α-$NaFeO_2$	Anomaly ($T_N < 1.8$ K)	−104	4.48	4.54

[a] Observed values at room temperature.
[b] Calculated values by Van Vleck formula [8].

where $\gamma = \lambda/K_BT$ is $\frac{1}{2l}$ of the ratio of the overall multiplet width to k_BT. By fitting this equation to the experimental magnetic susceptibility, the spin–orbit coupling constant λ is obtained to be 347(1) cm^{-1}. This value agrees well with the value in other oxides containing Eu^{3+}, for example, 327 cm^{-1} for $LiEuO_2$ [4], 332 cm^{-1} for Ba_2EuTaO_6 [9], and 323 cm^{-1} for $NaEuTiO_4$ [10].

Magnetic susceptibility measurements show that among the $NaLnO_2$ compounds, the Sm, Eu, Er (both the β-$LiFeO_2$ type and the α-$NaFeO_2$ type compounds), Tm, and Yb compounds are paramagnetic down to 1.8 K. The Weiss constants (θ) and the effective magnetic moments (μ_{eff}) have been calculated by fitting the Curie–Weiss law to the χ^{-1} vs. T plots. They are listed in Table 3. Figs. 4(a) and (b) show the temperature dependence of the reciprocal magnetic susceptibilities for $NaErO_2$ with the β-$LiFeO_2$ and the α-$NaFeO_2$ type structures. No much difference has been observed in their temperature dependences, the Weiss constants and the effective magnetic moments between the β-$LiFeO_2$ type and the α-$NaFeO_2$ type $NaErO_2$ compounds.

Figs. 5(a), 6(a) and 7(a) show the low-temperature susceptibilities for $NaLnO_2$ with Ln = Gd, Dy, and Ho, respectively. A peak in the magnetic susceptibility vs. temperature has been observed at 2.4 K for $NaGdO_2$, at 2.7 K for $NaDyO_2$ and at 2.4 K for $NaHoO_2$. These magnetic anomalies are attributable to the antiferromagnetic orderings of the Ln^{3+} moments in the $NaLnO_2$ compounds.

Fig. 8(a) shows the detailed temperature dependence of magnetic susceptibility for $NaNdO_2$ in the lower temperature region. The rapid increase of the magnetic susceptibility with decreasing temperature has been observed below 10 K. The Weiss constant calculated by fitting the Curie–Weiss law to the $\chi^{-1} - T$ curve between 4 and 10 K (see the inset of Fig. 8(a)) is 2.5 K. These results suggest that $NaNdO_2$ transforms to the ferromagnetic state below 2.4 K. To furthermore

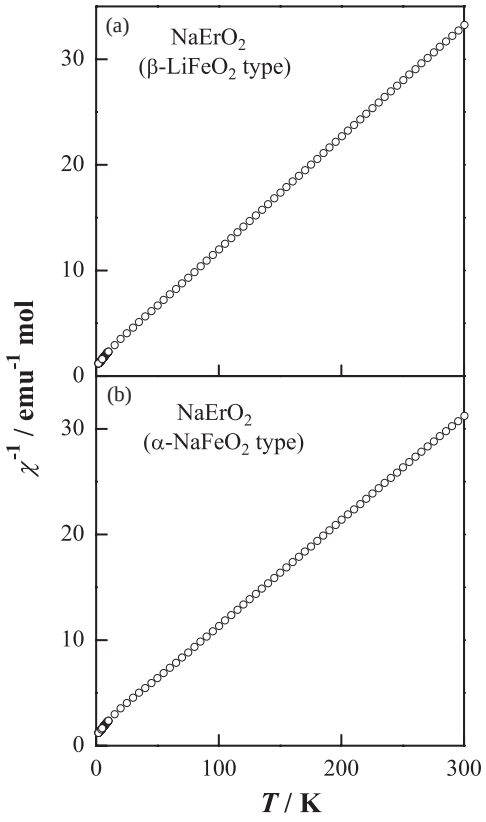

Fig. 4. Temperature dependences of the reciprocal magnetic susceptibilities for (a) $NaErO_2$ with the β-$LiFeO_2$ type structure and (b) $NaErO_2$ with the α-$NaFeO_2$ type structure.

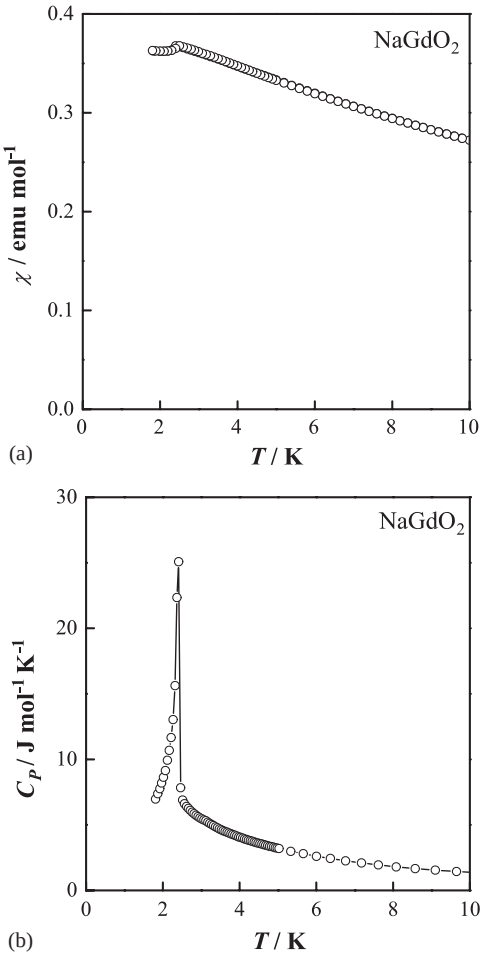

Fig. 5. The low-temperature dependences of (a) magnetic susceptibility and (b) specific heat for $NaGdO_2$.

investigate these magnetic anomalies, the magnetization measurements have been performed at 1.8, 3.0, and 5.0 K, and their results are shown in Fig. 9. At 5.0 K, no magnetic hysteresis loop has been observed and the magnetization is not saturated even in a magnetic field of 9 T. When the temperature is decreased down to 1.8 K, the data show the saturation magnetization to be $1.33\,\mu_B$, which indicates that the magnetic state of $NaNdO_2$ is ferromagnetic. Similar ferromagnetic behavior has been observed below 24 K for the other neodymium oxide $Ba_3NdRu_2O_9$ [11].

3.2.2. *Specific heats*

In order to furthermore investigate the magnetic transitions and the magnetic anomalies observed in the magnetic susceptibility measurements, the specific heats have been measured in the temperature range of $1.8 \leqslant T \leqslant 300$ K for all the $NaLnO_2$ compounds.

Figs. 5(b) and 7(b) show the temperature dependence of the specific heat (C_p) for $NaGdO_2$ and $NaHoO_2$ in the low temperature region ($1.8 \leqslant T \leqslant 300$ K). These C_p-T curves show a λ-type sharp anomaly at 2.4 K for both $NaGdO_2$ and $NaHoO_2$, which corresponds to the antiferromagnetic transition observed in their magnetic susceptibilities.

Fig. 6(b) shows the temperature dependence of the specific heat (C_p) for $NaDyO_2$ in the low temperature range. A sharp specific heat anomaly has been observed at 2.2 K, which corresponds to the antiferromagnetic interaction in the magnetic susceptibility vs. temperature curve. We will estimate the magnetic entropy change associated with the antiferromagnetic interaction from these specific heat data. The specific heat mainly consists of the lattice and magnetic specific heats. To estimate the lattice contribution, we used a polynominal function of the temperature, $f(T) = aT^3 + bT^5 + cT^7$, in which the constants were determined by fitting this function to the observed specific heat data between 25 and 40 K. The magnetic specific heat (C_{mag}) is obtained by subtracting the lattice contribution from the total specific heat, $C_{mag}(T) = C_p(T) - f(T)$. A dashed line in the C_p-T curve represents the extrapolated specific heat below 1.8 K. This is calculated by fitting the specific heat (almost the contribution of magnetic specific heat) to the function $f'(T) = a'T^3$ in the temperature range $1.8 \leqslant T \leqslant 2.2$ K, which is based on the antiferromagnetic spin-wave model [12]. The temperature dependence of

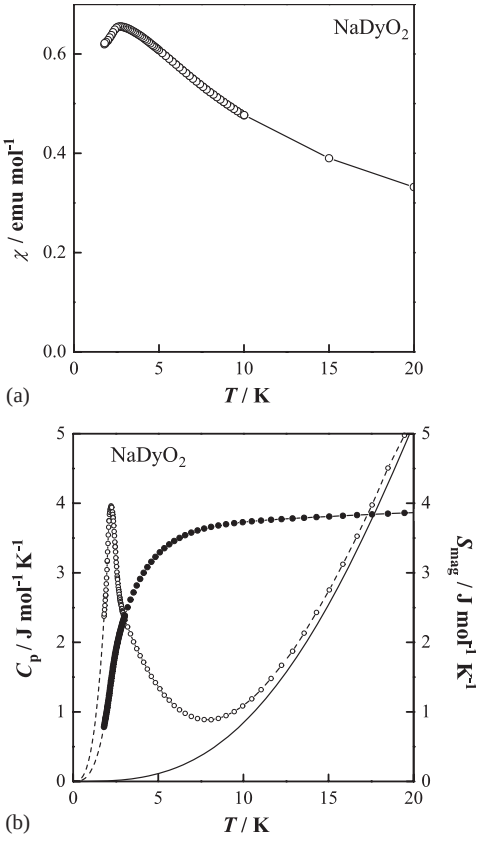

Fig. 6. (a) The low-temperature dependence of magnetic susceptibility for $NaDyO_2$. (b) Temperature dependences of the specific heat (left ordinate) and the magnetic entropy change (right ordinate) for $NaDyO_2$. The solid line in Fig. 6(b) is the calculation results for the lattice specific heat.

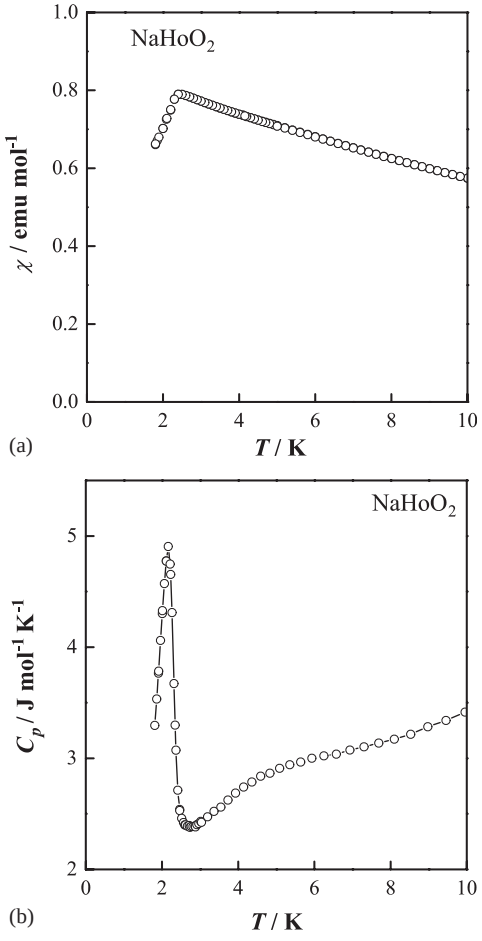

Fig. 7. The low-temperature dependences of (a) magnetic susceptibility and (b) specific heat for $NaHoO_2$.

the magnetic entropy calculated by $S_{mag} = \int (C_{mag}/T)\,dT$ is also shown in Fig. 6(b). From the $S_{mag} - T$ curve, the magnetic entropy change is estimated to be $\sim 4\,J\,mol^{-1}\,K^{-1}$. The ground state of Dy^{3+} is expected to split into eight doublets in the monoclinic symmetry C_2. The experimental value is a little smaller than the value expected for the ground Kramers' doublet, $R\ln 2 = 5.76\,J\,mol^{-1}\,K^{-1}$ (R: gas constant). This result may indicate that a short-range ordering of the Dy^{3+} magnetic moments begins above the antiferromagnetic transition temperature and a long-range antiferromagnetic ordering occurs at 2.2 K. The same behavior has been observed in $LiDyO_2$ [4].

Fig. 8(b) shows the temperature dependence of the specific heat for $NaNdO_2$ in the temperature range of $1.8 \leqslant T \leqslant 10$ K. A λ-type anomaly has been observed at 2.4 K in the $C_p - T$ curve, which corresponds to the magnetic anomaly found in the magnetic susceptibility vs. temperature curve.

Figs. 10(a)–(d) show the temperature dependences of the specific heat (C_p) in the low temperature region ($1.8 \leqslant T \leqslant 20$ K) for the Sm, Er (β-$LiFeO_2$ type), Tm, and Yb compounds, respectively. In the $NaTmO_2$ compound, the C_p has a broad peak at about 8.0 K, which should be attributed to a Schottky-like anomaly. The values of C_p for $NaSmO_2$, $NaErO_2$, and $NaYbO_2$ increase with decreasing temperature below 7.5, 5.0, and 12.0 K, respectively. The ground states, $^6H_{5/2}$ for the Sm^{3+} ion, $^4I_{15/2}$ for the Er^{3+} ion, and $^2F_{7/2}$ for the Yb^{3+} ion are expected to split into three doublets in the tetragonal symmetry D_{2d}, eight doublets in the monoclinic symmetry C_2, and four doublets in the rhombohedral symmetry D_{3d}, respectively. Thus, the anomalies in their specific heat at low temperatures are attributable to these low-lying Kramers' doublets, i.e., the magnetic ordering should occur at furthermore lower temperatures than 1.8 K. The large negative Weiss constants for these compounds listed in Table 3 are due to the antiferromagnetic interaction of these rare earth ions.

4. Conclusion

Table 3 summarizes the magnetic properties of $NaLnO_2$ prepared in this study. The Gd, Dy and Ho

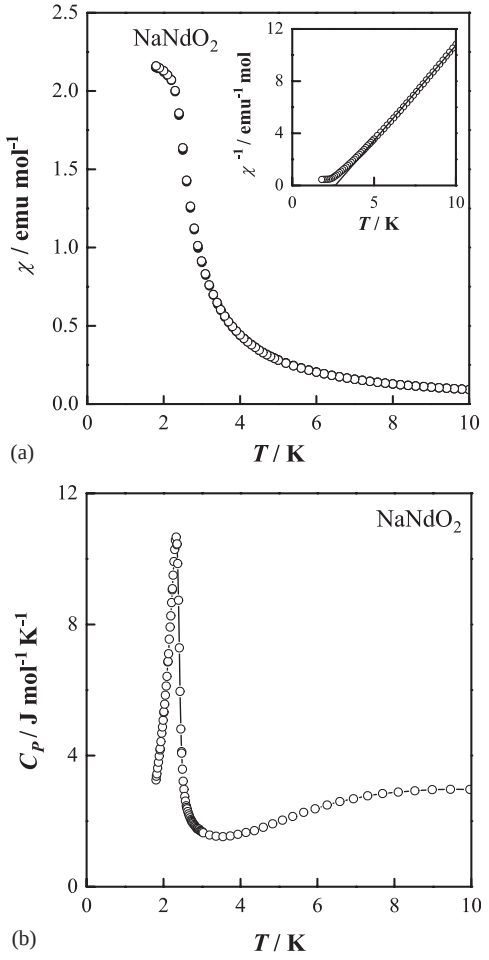

Fig. 8. (a) The low-temperature dependence of magnetic susceptibility for $NaNdO_2$. The inset shows the reciprocal magnetic susceptibility vs. temperature curve. (b) The low-temperature dependence of specific heat for $NaNdO_2$.

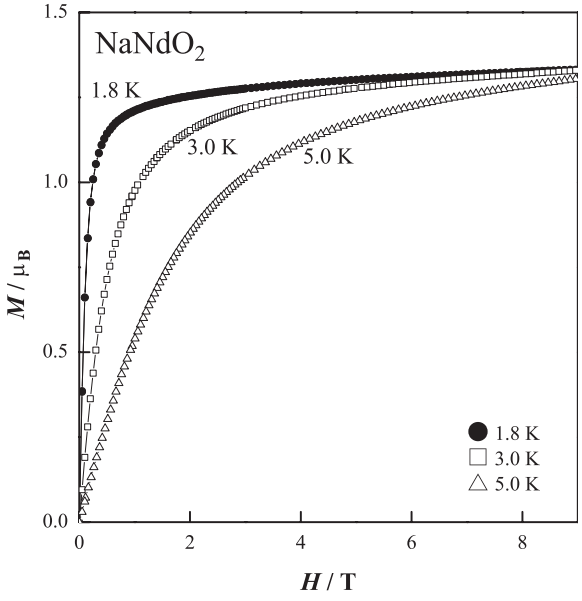

Fig. 9. Field dependence of the magnetization for $NaNdO_2$ at 1.8, 3.0, and 5.0 K.

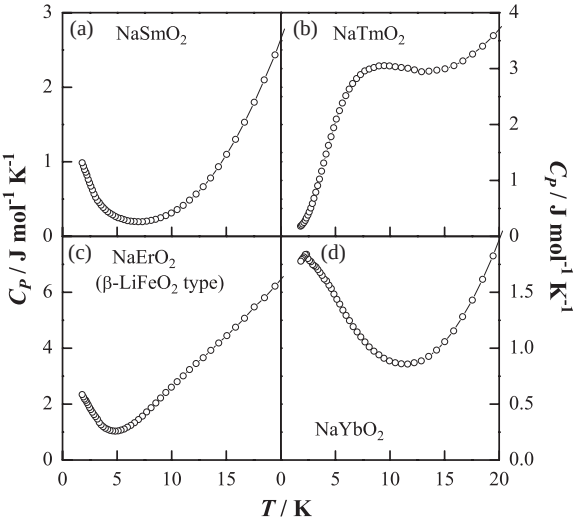

Fig. 10. Temperature dependences of the specific heat for (a) $NaSmO_2$, (b) $NaErO_2$ (β-$LiFeO_2$ type), (c) $NaTmO_2$, and (d) $NaYbO_2$ in the low temperature region ($1.8 \leqslant T \leqslant 20$ K).

compounds show an antiferromagnetic transition at low temperatures. $NaNdO_2$ transforms to the ferromagnetic state below 2.4 K. The Sm, Er, and Yb compounds exhibit a magnetic anomaly due to the antiferromagnetic ordering at furthermore lower temperatures (<1.8 K).

Acknowledgments

The authors are indebted to the Iketani Science and Technology Foundation for the financial support.

References

[1] R. Hoppe, S. Voigt, in: G. Meyer, L.R. Morss (Eds.), Synthesis of Lanthanide and Actinide Compounds, Klumer Academic Publisher, Netherlands, 1991, p. 225.
[2] H. Bergmann, Gmelin Handbuch, Teil C2 39 (1974) 114.
[3] M.D. Faucher, Ph. Sciau, J.-M. Kiat, M-G. Alves, F. Bouree, J. Solid State Chem. 137 (1998) 242.
[4] Y. Hashimoto, M. Wakeshima, K. Matsuhira, Y. Hinatsu, Y. Ishii, Chem. Mater. 14 (2002) 3245.
[5] G. Blasse, J. Inorg. Nucl. Chem. 28 (1966) 2444.
[6] M. Gondrand, M. Brunel, F. de Bernevin, Acta Crystallogr. B 28 (1972) 722.
[7] F. Izumi, T. Ikeda, Mater. Sci. Forum 321 (2000) 198.
[8] J.H. Van Vleck, The Theory of Electric and Magnetic Susceptibilities, Clarendon, Oxford, 1932.
[9] Y. Doi, Y. Hinatsu, J. Phys.: Condens. Matter 13 (2001) 4191.
[10] K. Tezuka, Y. Hinatsu, J. Solid State Chem. 138 (1998) 346.
[11] Y. Doi, Y. Hinatsu, Y. Shimojo, Y. Morii, J. Solid State Chem. 161 (2001) 113.
[12] Y.J. Tang, X.W. Cao, J.C. Ho, H.C. Ku, Phys. Rev. B 46 (1991) 1213.